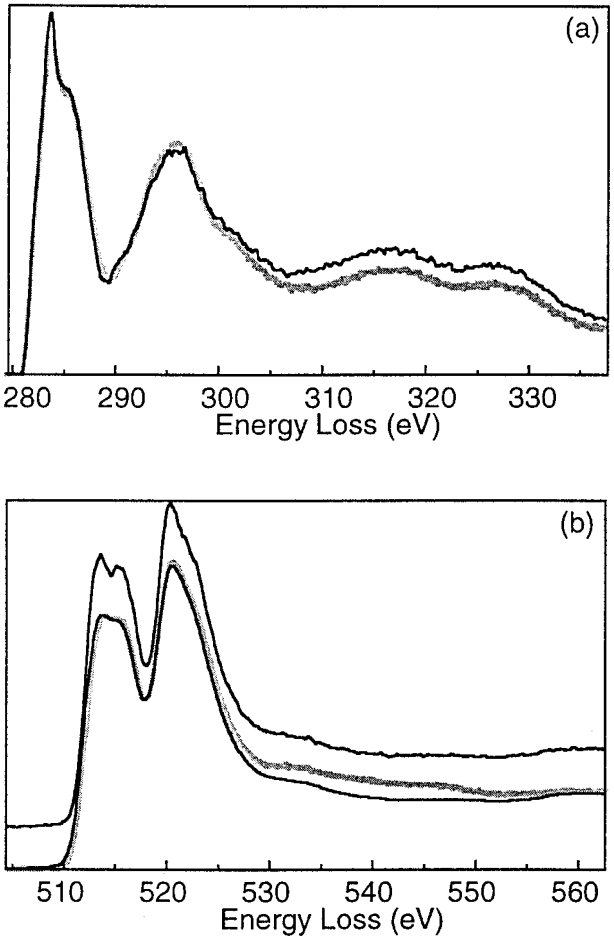

Fig. 2. a) Comparison of the C K-edge from a commercial VC powder (fine line, ~0.3 eV energy resolution) with that from V_8C_7 prepared by an SSM reaction (thick line, ~1 eV resolution). b) Comparison of the V $L_{2,3}$-edges. The two superimposed spectra have an energy resolution of ~1.6 eV while that displaced upward has an energy resolution of ~0.3 eV.

1.504 Å). Patterns were indexed using TREOR or METRIC-LS programs. SEM/EDX was carried out on a JEOL JSM820 microscope, equipped with a Kevex Quantum Detector Delta 4, and a Hitachi SEM S-570. Infrared spectra were recorded on a Nicolet 205 spectrometer using KBr pressed discs. Elemental compositions were determined by the departmental service using combustion in oxygen with tin powder as a combustion aid. The EELS spectra from the commercial VC powder (Alpha chemicals) were recorded using a GATAN 666 PEELS spectrometer on a VG Microscopes HB5 scanning transmission electron microscope operated at 100 keV, whereas those from the V_8C_7 produced by the SSM reaction were recorded using a similar spectrometer system on a Phillips CM20 transmission electron microscope with a field emission gun operated at 200 keV.

Reactions of Al_4C_3 and Transition Metal Halides ($TiCl_3$, $ZrCl_4$, VCl_3, WCl_4, $MoCl_3$, and $MoCl_5$): Transition metal halide, MX_n, and aluminum carbide, $n/12$ Al_4C_3 (0.1 mmol), were ground together and heated inside an evacuated ampoule. The ampoule was placed with 2/3 of its length inside a tube furnace at 500 °C. The reaction was left for 2–3 h at 500 °C and then the temperature was raised by 100 °C every 12 h to 1000 °C and left to anneal for 2–5 days. The coformed $AlCl_3$ separated from the black-gray carbide product by sublimation to the cool end of the ampoule.

The black or gray solids obtained were treated with THF (2 × 5 mL) and methanol (1 × 10 mL) and dried in vacuo. The resulting gray to black powders were analyzed using powder XRD (Table 1), SEM/EDX, FTIR, elemental microanalysis and, in the case of vanadium, PEELS. (Microanalysis: V_8C_7: Obs. C 13.75, H 0.21, N 0.19 %; Calcd. C = 17.07 %; Mo_2C: Obs. C 6.66, H 0.0, N 0.0 %; Calcd. C = 5.88 %; WC: Obs. C 6.64, H 0.14, N 0.0 %; Calcd. C = 6.12 %.)

Reactions of CaC_2 with $TiCl_3$, $ZrCl_4$, VCl_3, WCl_4, $MoCl_3$, and $MoCl_5$: Metal halide, MX_n, and calcium carbide, $n/2$ CaC_2 (0.2 mmol), were ground together and heated in an evacuated Pyrex glass ampoule. This induced a rapid reaction that produced a red glow at ca. 200–350 °C with the product spread along the inside walls of the ampoule. The temperature was ramped to 500 °C (20 °C/min), left for an hour, and allowed to cool to room temperature. The solids obtained were triturated with methanol (5 × 6 mL), dried in vacuo and analyzed by powder XRD (Table 1), SEM/EDX, and FTIR.

Received: January 23, 1998
Final version: March 9, 1998

[1] C. Marquez-Alvarez, J. B. Claridge, A. P. E. York, J. Sloan, M. L. H. Green, *Stud. Surf. Sci. Catal.* **1997**, *106*, 485.
[2] K. J. A. Brookes, *World Directory and Handbook of Hardmetals and Hard Materials*, 5th ed., International Carbide Data, East Barnet, Hertfordshire, UK **1992**.
[3] *Kirk-Othmer Encyclopedia of Chemical Technology*, 4th ed. (Ed: J. I. Kroschwitz), Wiley, Chichester **1992**, Vol. 4, p. 841.
[4] D. V. Baxter, M. H. Chisholm, G. J. Gama, V. F. Distasi, *Chem. Mater.* **1996**, *8*, 1222.
[5] D. V. Baxter, M. H. Chisholm, V. F. Distasi, S. T. Haubrich, *Chem. Mater.* **1995**, *7*, 84.
[6] I. P. Parkin, *Chem. Rev.* **1996**, 199.
[7] P. R. Bonneau, R. Jarvis, R. B. Kaner, *Nature* **1991**, *349*, 510.
[8] H. Goldsmidt, *Interstitial Alloys*, Butterworths, London **1967**, p. 92.
[9] A. J. Craven, *J. Microsc.* **1995,** *180*, 250.

Superlattices of Self-Assembled Tetrahedral Ag Nanocrystals**

By *Zhong L. Wang*,* *Steven A. Harfenist*, *Igor Vezmar*, *Robert L. Whetten*, *James Bentley*, *Neal D. Evans*, and *Kathy B. Alexander*

Size- and shape-selected passivated nanocrystals behave like molecular matter that can be used as the fundamental building blocks for constructing ordered arrays of metal, semiconductor, and ceramic nanocrystals.[1–11] The formation of self-assembled arrays involves the self-organization into monolayers, thin films, and/or superlattices of size-selected nanoclusters encapsulated in a compact protective organic coating. Nanocrystals can be arranged with long-range translational and even orientational order, forming a new state of materials with ordering on two different length scales: the atomic dimension and the nanocrystal molecular

[*] Prof. Z. L. Wang
School of Materials Science and Engineering
Georgia Institute of Technology
Atlanta, GA 30332-0245 (USA)
S. A. Harfenist, I. Vezmar, Prof. R. L. Whetten
School of Physics, Georgia Institute of Technology
Atlanta, GA 30332-0430 (USA)
Dr. J. Bentley, Dr. N. D. Evans, Dr. K. B. Alexander
Metals and Ceramics Division
Oak Ridge National Laboratory
Oak Ridge, TN 37831-6376 (USA)

[**] This research was partially sponsored by NSF grant DMR-9632823 and by the Division of Materials Sciences, US Department of Energy, under contract DE-AC05-96OR22464 with Lockheed Martin Energy Research Corp., and through the SHaRE Program under contract DE-AC05-76OR00033 with Oak Ridge Associated Universities.

  0935-9648/98/1007-0808 $ 17.50+.50/0

ADVANCED MATERIALS

dimension. With control of the interparticle distance by choosing the length of the passivation molecules, a transition from insulator to semiconductor or conductor is possible owing to strong interparticle interactions. This resonance gives rise to new plasmon modes, possibly leading to large optical nonlinearity.[12]

The crystallography of self-assembled nanocrystal superlattice (NCSs) materials can be strongly affected by the geometrical shape of the nanocrystals, because the interaction between adjacent nanocrystals is believed to be weak (van der Waals forces) so that the packing is determined, to a large extent, by the geometrical configuration.[13] In this communication, we report the successful preparation of well-ordered arrays of Ag nanocrystals whose predominant shape is tetrahedral. The packing exhibits not only long-range translational order but also short-range orientational order. A model is suggested to interpret the geometrical packing of the nanocrystals and the conclusion supports the bundling of passivation molecules on nanocrystal surfaces.

Silver nanocrystals with specific size and shape were synthesized by an aerosol technique, reported in detail elsewhere.[6,14] The nanocrystals were passivated by $SC_{12}H_{25}$ chain molecules and were suspended in toluene. Ordered NCSs were formed by slowly drying a droplet of the solution on a thin carbon (or SiO_x) film supported by a copper grid. The structure of the nanocrystals was determined using transmission electron microscopy (TEM). The TEM experiments were performed at 300 kV using a Philips CM30 TEM and at 400 kV using a JEOL 4000EX high-resolution TEM.

For imaging the ordered distribution of nanocrystals, conical scan dark-field TEM imaging, obtained in the dark-field mode with a centered objective aperture while the incident beam is tilted and scanned conically,[15] has shown great potential for distinguishing monolayer, bilayer, and trilayer NCSs. Figure 1 is a dark-field TEM image of a monolayer Ag NCS, which clearly shows the size uniformity of the nanocrystals. The slight contrast variation among particles is due to their relative orientations. The distribution of the nanocrystals has a 2*m* symmetry that is likely to be due to the shape of the nanocrystals, as discussed below. Dark-field imaging is useful for illustrating the particle core distribution but is a difficult method for determining the particle shape owing to nanocrystal wobbling under the beam during the long exposure time needed to record the image, typically ~10 s.

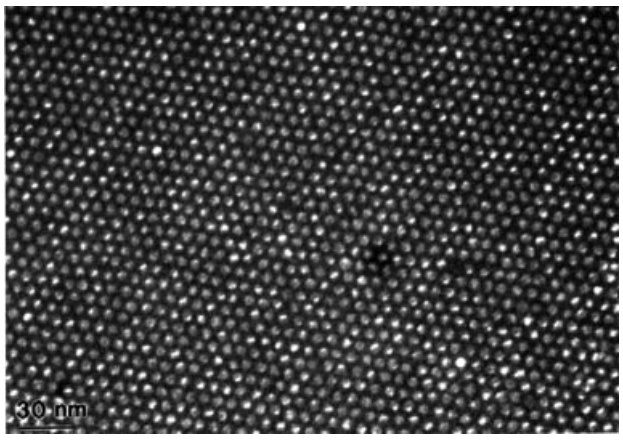

Fig. 1. Dark-field TEM image of Ag nanocrystals, passivated with thiolates and dispersed on carbon film, showing ordered self-assembly with long-

Figure 2a shows a bright-field TEM image of a near-complete monolayer Ag NCS, where more than 70 % of the particles can be identified to have a triangular projected shape. The small-angle electron diffraction pattern shown in the inset proves the ordered structure. There are two possible geometrical configurations that are likely to give the projected triangular shapes in the nanocrystal system, one is a tetrahedron bounded by four {111} facets, the other is a (111) based platelet structure. If the latter were the structure seen here, the contrast within each nanocrystal in the dark-field image would be uniform because of the uniform thickness of the nanocrystal. In contrast, the dark-field TEM image given in Figure 2b from the same specimen area clearly shows that the contrast across each nanocrystal is non-uniform, as there is a small bright dot within the projected area of each nanocrystal. This suggests that the nanocrystals have a pyramidal shape, where the white dot corresponds to the projected position of the vertical apex of the tetrahedron, simply because the contrast in the dark-field image is directly related to the projected mass thickness if the diffraction effect is ignored. A high-resolution TEM image of the nanocrystals, as shown in the inset in Figure 2b, also proves the tetrahedral shape of the particle, where the incident beam direction is [110], along which two {111} faces are imaged edge-on. It is also noticed that the apexes of the nanocrystals appear to be truncated, possibly because the atoms at the apexes have higher energy and they are likely to move to sites having lower energy.[16] The low-angle electron diffraction pattern clearly indicates the ordered assembly of the nanocrystals, while the pattern gives a 2*m* symmetry rather than 3*m*. This is important evidence for constructing the geometrical model of the NCS.

To further confirm the tetrahedral shape of the nanocrystals, the specimen was tilted by ~40° in the TEM. From the TEM image shown in Figure 3 most of the particles still have a projected triangle shape, as expected. The decrease in the interplanar distance in the horizontal direction is a foreshortening effect due to the tilt of the specimen.

The data presented above unambiguously show the long-range translational order of the NCSs. Two important questions are of particular interest. They concern the orientational ordering of the nanocrystals and the geometrical pattern of the self-assembly. The images shown in Figure 2 indicate that the orientation of the nanocrystals is close to uni-axial along the normal direction of the substrate, but the in-plane twisting may only have short-range order. To answer these questions, we first examine an ideal situation

  0935-9648/98/1007-0809 $ 17.50+.50/0

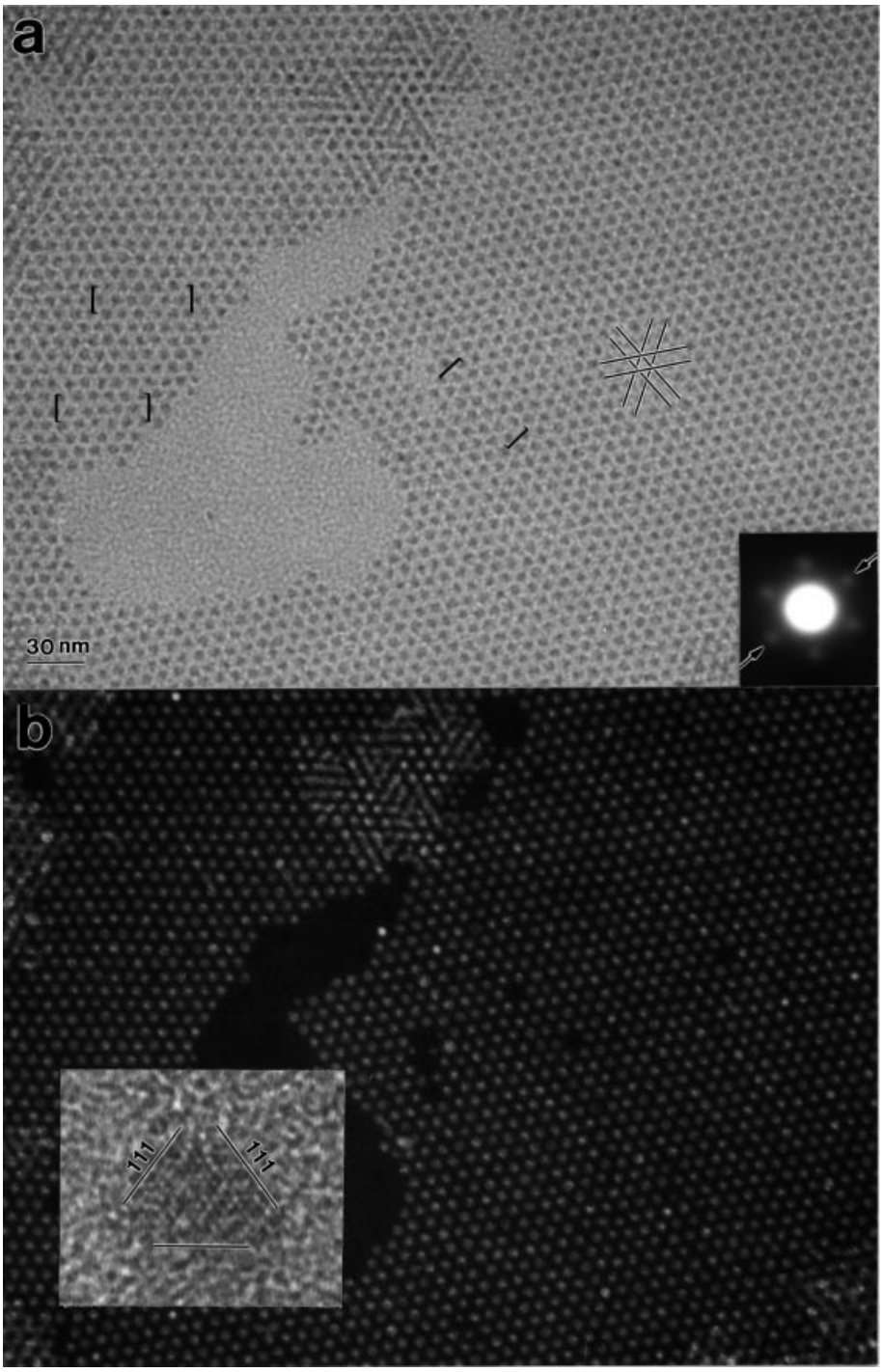

Fig. 2. a) Bright-field and b) dark-field TEM image of a monolayer assembled superlattice of tetrahedral Ag nanocrystals. A low-angle electron diffraction pattern is inserted in (a), corresponding to the interplanar distances indicated in the images. A high-resolution TEM image of a tetrahedral Ag nanocrystal is shown in the inset of (b), whose shape is a truncated tetrahedron because the atoms located near the apexes are absent.

for the geometrical assembly of identical tetrahedra. A few possible configurations are proposed in Figure 4. These models are given based on two theoretical predictions:[17] the adsorbate heads are tethered uniformly to the nanocrystal surfaces but the chain-like tails are packed into bundles to give the lowest energy. The experimental observation of truncated octahedral Ag nanocrystals supports these two predictions.[6] If the perfect three-fold symmetry is preserved, the model shown in Figure 4a would be the choice, but this model leave unfilled space (an array of large voids) in the monolayer. The model shown in Figure 4b is also similarly unfavored. The model presented in Figure 4c fills the space. A careful examination of this model gives three nanocrystal lines, two of which are of equal interplanar distance, while the third one is slightly smaller than the other two, exhibiting two-fold mirror symmetry. The real-space symmetry of this model agrees well with the experimentally observed low-angle electron dif-

  0935-9648/98/1007-0810 $ 17.50+.50/0

ADVANCED MATERIALS

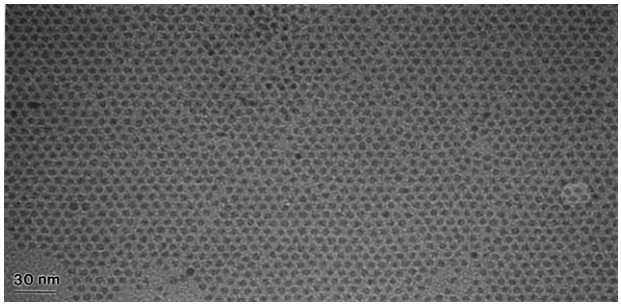

Fig. 3. Bright-field TEM image of a monolayer Ag NCS after the specimen was tilted by 40°.

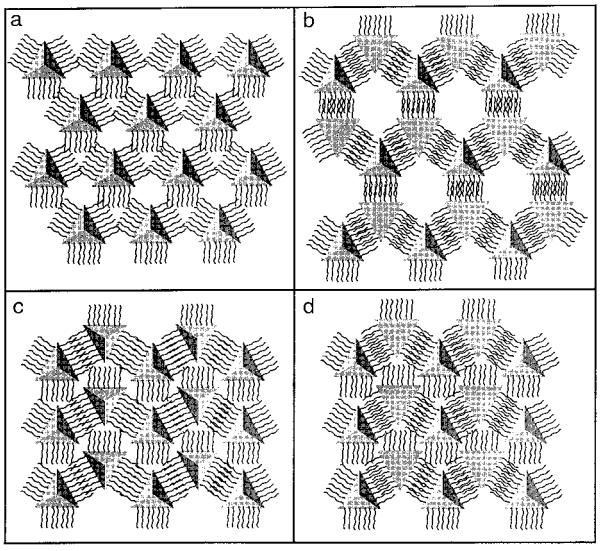

Fig. 4. a–d) Possible monolayer self-assembly models of tetrahedral nanocrystals passivated by bundled thiolate molecules.

fraction pattern inserted in Figure 2a, in which the scattering angle of one pair of planes (indicated by arrowheads) is larger than the angles of the other two sets of planes (2*m* symmetry). More directly, the real-space distribution of the tetrahedral particles in some regions, as indicated in Figure 2a, agrees with this model. Therefore, model c in Figure 4 is likely to be a good illustration of the orientationally ordered packing of the tetrahedral nanocrystals. Alternatively, the model given in Figure 4d shows the same characteristics as the one in Figure 4c, but half of the particles face down to produce the most compact packing, as required for minimizing the assembling energy. Unfortunately, the TEM images cannot distinguish model c from model d because of the results of projection.

To directly image the distribution of thiolate molecules on the particle surface, energy filtered electron images were acquired by selecting the electrons that excited the carbon K ionization edge in the TEM; the image intensity is proportional to the local projected density of carbon atoms. This is the so-called energy-filtered TEM (EF-TEM),[18] and a resolution of ~2 nm can be achieved. Figure 5 shows the bright-field TEM image and the corresponding EF-TEM image acquired by selecting the carbon K ionization edge using the electron energy filtering system equipped on the TEM. The dark spots correspond to the Ag nanoparticles, while the bright contrast areas represent higher local projected carbon concentrations, in which the effect from SiO_x substrate was removed by image processing. It is apparent that the distribution of carbon around the Ag nanocrystals is non-uniform, rather forming accumulated carbon-rich aggregates, in correspondence to the bundled thiolates on the particle surfaces.

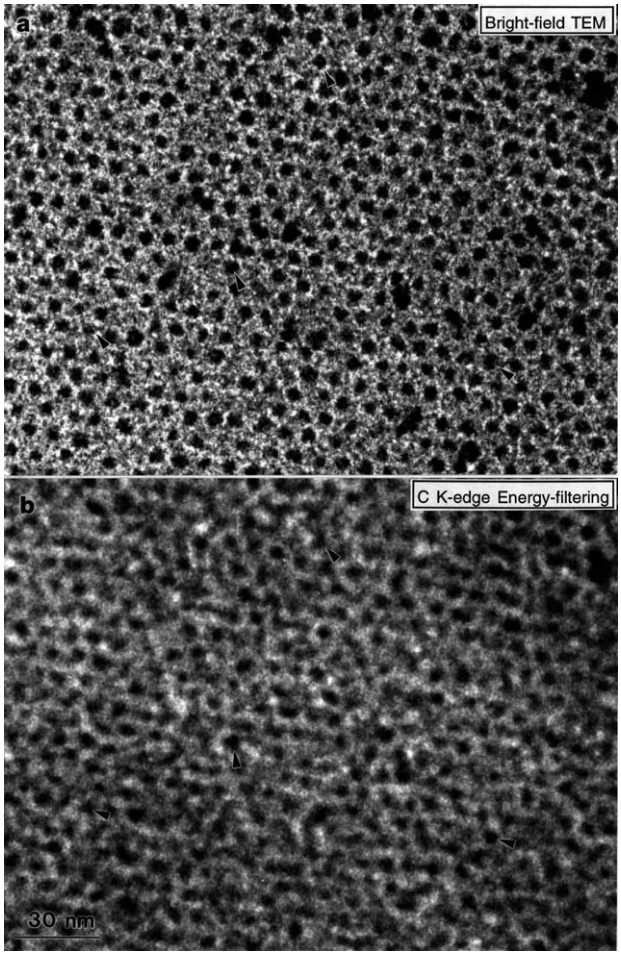

Fig. 5. a) Bright-field TEM image and b) energy filtered TEM image of electrons after exciting the carbon K edge, showing the distribution of carbon atoms around the nanocrystals. The arrowheads indicate a few nanocrystals around which the image contrast shows a trio-split, possibly indicating the bundling of passivation molecules on the surfaces of the nanocrystals.

In conclusion, tetrahedral Ag nanocrystals synthesized by an aerosol method behave like molecular matter, forming patterned nanocrystal superlattices (NCSs). The NCSs have long-range translational order, while the orientational order is short range. A model is suggested to explain the observed orientational order and the results support the following: the thiolate adsorbates are distributed over the nanocrystal surfaces, their extended tails (chains) extend to

  0935-9648/98/1007-0811 $ 17.50+.50/0

form bundles, and the entire assemblies orient in such a way that the bundles tend to fill the entire space.

Received: January 19, 1998

[1] M. D. Bentzon, J. Van Wonterghem, S. Mørup, A. Thölen, C. J. W. Koch, *Philos. Mag. B* **1989**, *60*, 169.
[2] C. B. Murray, C. R. Kagan, M. G. Bawendi, *Science* **1995**, *270*, 1335.
[3] R. L. Whetten, J. T. Khoury, M. M. Alvarez, S. Murthy, I. Vezmar, Z. L. Wang, C. C. Cleveland, W. D. Luedtke, U. Landman, *Adv. Mater.* **1996**, *8*, 428.
[4] J. Dorogi, J. Gomez, R. Osifchin, R. P. Andres, R. Refenberger, *Phys. Rev. B* **1995**, *52*, 9071.
[5] R. P. Andres, T. Bein, M. Dorogi, S. Feng, J. I. Henderson, C. P. Kubiak, W. Mahoney, R. G. Osifchin, R. Reifenberger, *Science* **1996**, *273*, 1690.
[6] S. A. Harfenist, Z. L. Wang, M. M. Alvarez, I. Vezmar, R. L. Whetten, *J. Phys. Chem.* **1996**, *100*, 13 904. S. A. Harfenist, Z. L. Wang, M. M. Alvarez, I. Vezmar, R. L. Whetten, *Adv. Mater.* **1997**, *9*, 817.
[7] J. R. Heath, C. M. Knobler, D. V. Leff, *J. Phys. Chem. B* **1997**, *101*, 189.
[8] A. P. Alivisatos, *Science* **1996**, *271*, 933.
[9] L. Motte, F. Billoudet, E. Lacaze, M.-P. Pileni, *Adv. Mater.* **1996**, *8*, 1018.
[10] S. I. Stupp, V. Le Bonheur, K. Walker, L. S. Li, K. E. Huggins, M. Kerser, A. Amstutz, *Science* **1997**, *276*, 384.
[11] J. S. Yin, Z. L. Wang, *Phys. Rev. Lett.* **1997**, *79*, 2570.
[12] C. P. Collier, R. J. Saykally, J. J. Shiang, S. E. Henrichs, J. R. Heath, *Science* **1997**, *277*, 1978.
[13] Z. L. Wang, *Adv. Mater.* **1998**, *10*, 13.
[14] M. M. Alvarez, I. Vezmar, R. L. Whetten, *J. Aerosol Sci.*, in press.
[15] Z. L. Wang, *Ultramicroscopy* **1993**, *53*, 73.
[16] J. S. Yin, Z. L. Wang, unpublished.
[17] W. D. Luedtke, U. Landman, *J. Phys. Chem.* **1996**, *100*, 13 323.
[18] See: *Energy-Filtering Transmission Electron Microsocpy* (Ed: L. Reimer), Springer Series in Optical Sciences, Vol. 71, Springer, Berlin **1995**.

Surfactant-Assisted Synthesis of a Mesoporous Form of Zirconium Phosphate with Acidic Properties**

By *José Jiménez-Jiménez*, *Pedro Maireles-Torres*,* *Pascual Olivera-Pastor*, *Enrique Rodríguez-Castellón*, *Antonio Jiménez-López*, *Deborah J. Jones*, and *Jacques Rozière**

The continuous demand for acidic solids for use in the fields of catalysis and sorption has greatly encouraged the search for new materials with a porosity and intrinsic reactivity that can be tailored.[1] The synthesis of the family of M41S solids has shown that surfactant species favor, by a mechanism of cooperative nucleation, the formation of organo-inorganic nanocomposite biphase arrays, the structures of which mimic those of liquid crystals.[2,3] This synthetic approach is demonstrating its importance by its versatility, and a great variety of mesoporous solids have been prepared since the landmark articles of Beck et al. We report here the sol-gel synthesis of zirconium phosphate in the presence of a structure-directing cationic surfactant, leading to mesoporous solids with a BET (Brunauer–Emmett–Teller) surface area of ca. 250–320 $m^2 g^{-1}$ and a high and modulable surface acidity following removal of the surfactant by acid–ethanol extraction or by calcination at 540 °C.

Zirconium phosphate is the most studied member of the well-known family of layered solid acids.[4] "Pillared" derivatives can be prepared by intercalation of inorganic or organometallic species followed by a grafting reaction designed to eliminate organic matter, dehydroxylate, and anchor the pillaring metal oxide nanoparticle formed to the layer. These multifunctional zeolite-like compounds are meso- and microporous, and have potential applications as catalysts and catalyst supports.[5] Although templated syntheses of open-framework phosphates has been developed as a route to ultra-large pore solids,[6] until very recently, surfactant-assisted syntheses of metal phosphates led only to layered phases,[7] and the synthesis of mesoporous phosphate-based solids with pore dimensions larger than those of the aluminum phosphates remained a challenge. Last year, however, Zhao et al. reported the preparation of a thermally stable mesoporous hexagonal aluminophosphate and silicoaluminophosphate with BET surface areas of 772 and 928 $m^2 g^{-1}$, respectively.[8] Some months earlier, Ciesla et al. had recourse to phosphoric acid treatment of a surfactant-containing zirconium oxosulfate gel, which, by neutralizing the remaining ZrOH groups, helped to avoid the structural collapse of the zirconium oxide on removal of the surfactant. This led to high surface area zirconium oxophosphate.[9] In a different approach, we have used phosphoric acid directly at the stage of the formation of the inorganic matrix, and now report the templated synthesis and characterization of a new mesoporous zirconium phosphate with uniform pore dimensions and acidic properties.

The synthesis of this new templated zirconium phosphate (t-ZrP) was carried out by mixing an aqueous solution of cetyltrimethylammonium (CTMA) bromide (25 wt.-%, Aldrich) with orthophosphoric acid (85 wt.-%, BDH Analar) (P/CTMA molar ratio = 1). The CTMA solution was then aged for at least 30 min before adding zirconium *n*-propoxide ($Zr(OC_3H_7)_4$, 70 wt.-% solution in 1-propanol, Aldrich), in a molar ratio P/Zr = 2. The gel that immediately forms was stirred at room temperature for 2–3 days. The solid was then recovered by filtration, washed with ethanol, and dried at 60 °C. Two procedures were used to remove the surfactant: i) extraction with HCl/ethanol (ext-t-ZrP) and ii) calcination at 540 °C in air (calc-t-ZrP).

[*] Dr. P. Maireles-Torres, J. Jiménez-Jiménez, Prof. P. Olivera-Pastor, Prof. E. Rodríguez-Castellón, Prof. A. Jiménez-López
Departamento de Química Inorgánica, Cristalografía y Mineralogía
Universidad de Málaga
Campus de Teatinos, E-29071 Málaga (Spain)
Prof. J. Rozière, Dr. D. J. Jones
Laboratoire des Agrégats Moléculaires et Matériaux Inorganiques
ESA CNRS 5072, Université Montpellier 2
F-34095 Montpellier Cedex 5 (France)

[**] This research was funded in part by the CICYT (Spain) Project MAT 97-906.

  0935-9648/98/1007-0812 $ 17.50+.50/0